



Impact of tropical cyclones on the evolution of the monsoon-driven upwelling system in the coastal waters of the northern South China Sea

Binxin Zheng^{1,2} · Yunhai Li²  · Jiufa Li¹ · Fangfang Shu² · Jia He²

Received: 25 January 2017 / Accepted: 6 December 2017 / Published online: 19 December 2017
© Springer-Verlag GmbH Germany, part of Springer Nature 2017

Abstract

An upwelling system exists in the coastal waters of the northern South China Sea (NSCS), a region that is frequently affected by tropical cyclones in summer. This study investigates the evolution of the NSCS monsoon-driven upwelling system and the effects of the Talim and Doksuri tropical cyclones on the system using in situ observational data obtained at three mooring stations, one land-based meteorological station, and concurrent satellite remote sensing data for the NSCS coastal waters from May to July 2012. The results show that the occurrence and evolution of the upwelling system were mainly controlled by the Asian southwest monsoon, while the eastward current also made important contributions to the upwelling intensity. A decrease in the bottom water temperature and shifts in the along-shore and cross-shore currents were direct evidence of the establishment, existence, and recovery of this upwelling. Tropical cyclones have significant impacts on hydrodynamics and can thus influence the evolution of the NSCS upwelling system by changing the local wind and current fields. Variations in water level and local current systems impeded the development of upwelling during tropical cyclones Talim and Doksuri in the study area, which have low-frequency fluctuations of approximately 2–10 days. These variations were the results of the coupled interactions between local wind fields, coastal trapped waves, and other factors. The hydrodynamic environment of the marine water (including coastal upwelling system) rapidly recovered to normal sea conditions after each cyclone passed due to the relatively short duration of the impact of a tropical cyclone on the dynamic environment of the waters.

Keywords Tropical cyclone · Upwelling · Mooring observation · South China Sea

1 Introduction

Upwelling systems, which are affected by the topography of the seafloor (Allen 1973; Gan and Allen 2002; Gan et al. 2005; Gu et al. 2012), wind stress (Arthur 1965; Pringle 2002; Wang et al. 2014; Chen et al. 2014), and tidal mixing (Tee et al. 1993; Lü et al. 2008), bring relatively cool, deep (bottom) seawater with relatively high dissolved oxygen to the upper ocean. Upwelling has a significant influence on the marine ecological functions, ocean dynamics, local climate, and material cycle in the waters

where they exist (Gan and Allen 2002; Shang et al. 2004; Lu et al. 2010; Mazzini and Barth 2013), which is best proven by the fact that the majority of highly productive fisheries mainly exist in upwelling regions across the globe (Fréon et al. 2009).

The South China Sea (SCS) is one of the largest marginal seas of the West Pacific Ocean. There are a number of typical upwelling systems in the SCS, such as the upwelling system in the coastal area of the northern South China Sea (NSCS) (Gan and Allen 2002; Jiang et al. 2011; Gu et al. 2012; Wang et al. 2014; Hu and Wang 2016), the upwelling system over the southeast continental shelf off Hainan Island (Jing et al. 2009; Su et al. 2011), China, and the upwelling system over the continental shelf southeast of the Vietnam coast (Kuo et al. 2004; Hein et al. 2013). These upwelling systems play an important role in the evolution of the marine ecological environment. Research on the dynamic mechanisms by which an upwelling system is formed and evolved is the basis for accurately understanding and evaluating the impact of upwelling systems on the marine environment.

A typical seasonal upwelling system exists in the coastal area of the NSCS. Extensive field observations and modeling

Responsible Editor: Aida Alvera-Azcarate

✉ Yunhai Li
liyunhai@tio.org.cn

¹ State Key Laboratory of Estuarine and Coastal Research, East China Normal University, Shanghai, China

² Laboratory of Coast & Ocean Environmental Geology, Third Institute of Oceanography, SOA, Xiamen 361005, China

studies have been conducted to investigate the formation mechanism, evolution, and marine ecological effects of this upwelling system. The results show that the formation, maintenance, and evolution of this upwelling system were controlled by complex interactions between wind stress, topography, and ocean currents (including the Pearl River diluted water), and the upwelling system has significant impacts on the marine ecological environment, such as primary production enhancement (Cai and Lennon 1988; Gan et al. 2009a, b; Jiang et al. 2011; Gu et al. 2012; Wang et al. 2014; Gan et al. 2015). At the same time, the NSCS is a tropical cyclone-active area. On average, 2–3 tropical cyclones affect this area each year (Wang et al. 2009). Tropical cyclones impose one of the most intense air-sea interactions on the weather scale and can, together with strong winds and heavy rainfall, simultaneously significantly alter and affect the marine hydrodynamic environment (Chen et al. 2003; Zhang et al. 2009; Chang et al. 2010; Lin et al. 2010; Zhang et al. 2013; Li et al. 2015b) and marine biological and ecological systems (Zheng and Tang 2007; Chung et al. 2012). The strong dynamic environment accompanying tropical cyclones can alter and affect the current field structure of the waters within a short period of time, and it can also affect the development and evolution of the upwelling. Therefore, the upwelling region in the coastal area of the NSCS is a natural laboratory for conducting research on the effect of tropical cyclones on an upwelling system.

A tropical cyclone is accompanied by high cyclonic wind stress and heavy rainfall. The high cyclonic wind stress significantly increases the heat exchange between the air and sea (Niiler 1969; Jaimes and Shay 2015; Jaimes et al. 2016), mixes the upper and lower shallow coastal waters, and can cause an upward rise of bottom water. In addition, heavy rainfall decreases the salinity of the surface seawater and thus alters the temperature-salinity structure of the water (Chang et al. 2008; Li et al. 2013) and the coastal ecosystem (Tang et al. 2002; Hong et al. 2009). In shallow coastal waters, the strong dynamic process of a tropical cyclone stirs the seawater, resulting in the complete mixing of the waters, which may completely destroy the original water structure and current field (Li et al. 2012, 2013). These influences from tropical cyclones vary significantly with their different origins, paths, speeds, and intensities. However, because of the difficulty in accurately predicting the paths of tropical cyclones and the harsh observation conditions during storms, observations and investigations of the impact on the hydrodynamic environment by tropical cyclones are performed far less frequently than those for normal hydrodynamic processes. This issue requires urgent in-depth examination.

This study selects the monsoon-driven upwelling system in the coastal area of the NSCS to investigate the influences of tropical cyclones on upwelling, as this region was affected by two such events, namely, tropical cyclones Talim and Doksuri. Continuous hydrodynamic and meteorological data were collected during an approximately 80-day period (from May 14

to July 3, 2012) along with satellite remote sensing data. This paper is structured as follows. Section 2 introduces the background of the present study, which mainly includes information about the study area, evolution of the upwelling in the coastal area of the NSCS and the two tropical cyclones. Section 3 details the observation methods and data processing. Section 4 shows the research results, including the observations of hydrodynamic conditions and the influences of the two tropical cyclones. Section 5 discusses the influence of the tropical cyclones on the upwelling system in the study area and its dynamic mechanism. Section 6 presents the conclusions.

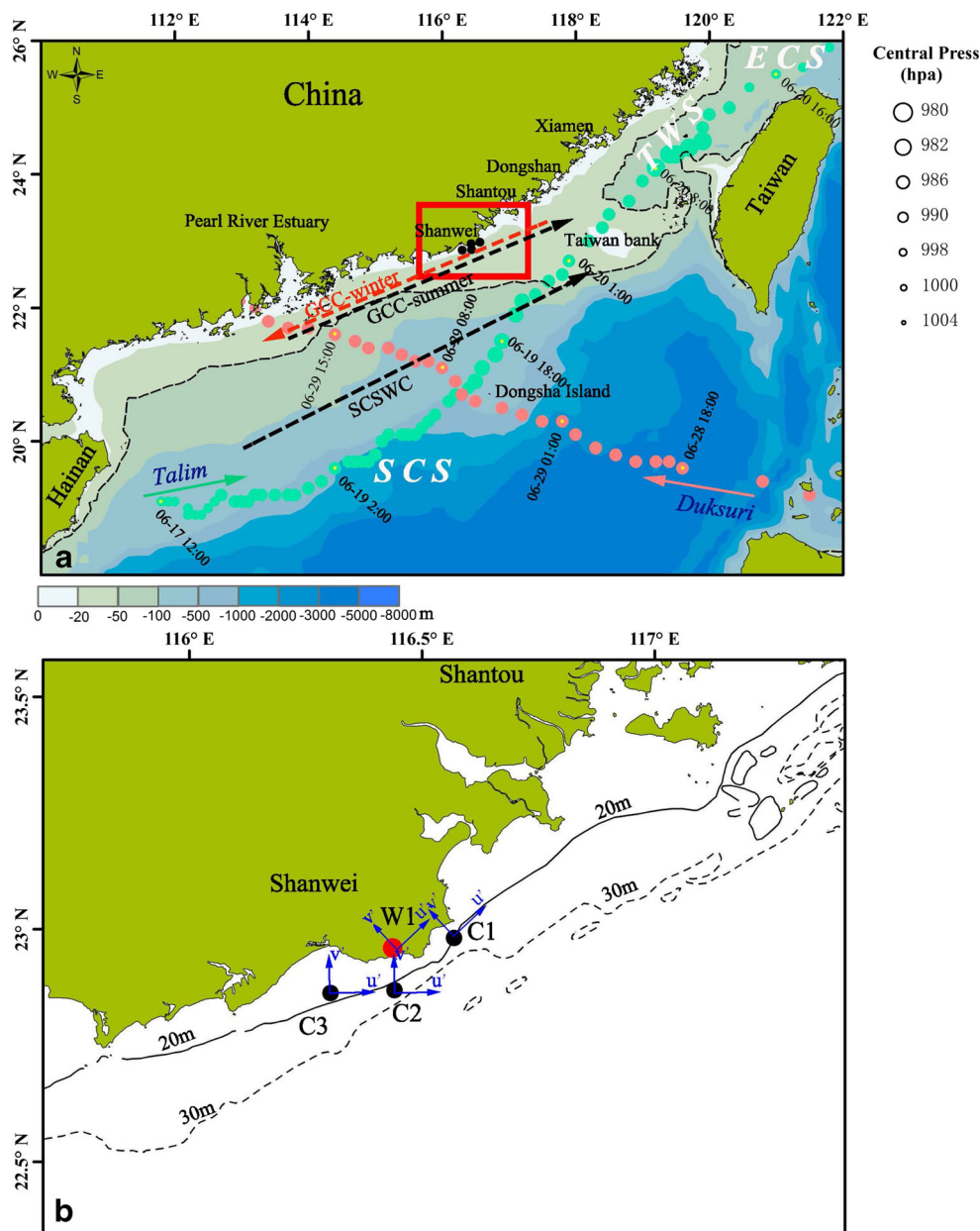
2 Background

2.1 Upwelling in the coastal areas of the NSCS

The coastal regions of the NSCS feature a tortuous and irregular coastline, a wide and shallow continental shelf and a complex topography. The circulation system in the NSCS includes the Guangdong coastal current, which flows northeastward in summer and southwestward in winter due to monsoons (Hu et al. 2000; Yang et al. 2002; Su 2004); the warm current of the SCS, which perennially flows northeastward along the continental shelf break (between the 100- and 200-m isobaths off the Guangdong coast) and extends to the Taiwan Strait (Chao et al. 1995; Xue et al. 2004; Guan and Fang 2006; Wang et al. 2010); and the Pearl River diluted water (Gan et al. 2009b) (Fig. 1a). Under the combined effects of the seasonal current field, wind stress, and seafloor topography, the surface water is transported away from the shore, and the bottom water rises along the seafloor towards the coast; as a result, an upwelling is formed. Among all the influence factors, the Asian southwest monsoon is the dominant factor in the formation of the upwelling (Hong et al. 2009; Jing et al. 2009; Zhang et al. 2011). Topography also plays an important role in the upwelling intensity in the NSCS (Gan et al. 2009a; Wang et al. 2014; Gan et al. 2015). Furthermore, ocean currents beyond the continental shelf and the Pearl River plumes considerably modulate the along-shore and cross-shelf upwelling circulation in the upper water column. These three processes have significant influences on the formation of the upwelling (Gan et al. 2009b).

The NSCS is located in a tropical cyclone-active area of the West Pacific Ocean (Chung et al. 2012). According to statistical data collected at the Shanwei Ocean Station (Fig. 1), between 1949 and 2008, there were an average of 2.6 (with a maximum of 9) tropical cyclones passing by the study area each year. Tropical cyclones mainly occur between June and September at the same time as when the upwelling in the coastal waters of the NSCS is developed (mainly from June to August). Due to the adverse weather and sea conditions during the tropical cyclones, scarce studies have been conducted to investigate how the upwelling system rapidly

Fig. 1 **a** Topographic map of the NSCS (GCC signifies the Guangdong Coastal Currents; SCSWC signifies the Warm Current of the South China Sea; the red box signifies the study area; SCS, ECS and TWS signify the South China Sea, the East China Sea and the Taiwan Strait, respectively; and green and red dots signify the paths of tropical cyclones Talim and Doksuri, respectively). **b** Topographic map of the study area (black dots signify the location of each bottom-supported seabed base observation station (C1, C2 and C3); the red dot signifies the location of the land meteorological observation station (W1); and the abscissa axis and ordinate axis of the coordinate system of stations C1, C2, C3 and W1 are along the shore (u') and perpendicular to the shore (v'), respectively). **c** The 20-m and 30-m contour lines



responds to tropical cyclones in the coastal area of the NSCS (Lin et al. 2003; Pan et al. 2012). Long-time seabed-based observations and remote sensing data are important methods that are urgently needed to study the impact of tropical cyclones on the evolution of the upwelling system.

2.2 Tropical cyclones Talim and Doksuri

Tropical cyclone Talim formed to the east of Hainan Island in the SCS on June 17, 2012 and intensified to a tropical storm (TS). Talim moved northeastward nearly parallel to the coast and reached the south side of the study area at approximately 12:00 on June 19 (UTC), when the storm intensified to a severe tropical storm (STS) with a maximum wind speed of 25 m/s, a

central pressure of 985 hPa and a level 7 wind circle of 200 km. The center of the storm was approximately 115 km south of the study area at this time. The level 7 wind circle radius continually covered the study area (Fig. 1a) until the storm moved north-eastward into the Taiwan Strait at 02:00 on June 20 (UTC). As Talim moved away from the study area, its influence on the study area gradually dissipated (Fig. 1a). The duration of Talim’s influence on the study area was approximately 2–3 days.

Tropical cyclone Doksuri formed in the West Pacific Ocean to the east of the Philippines. After it formed, Doksuri intensified to a tropical storm (TS) and passed through the Bashi Channel and then moved northwestward to the NSCS. Doksuri reached the southern region of the study area at 04:00 on June 29 (UTC), when the storm intensified to a

severe tropical storm (STS) with a maximum wind speed of 25 m/s, a central pressure of 985 hPa and a level 7 wind circle of 150 km. The storm center was approximately 220 km south of the study area at this time (Fig. 1a). Doksuri made landfall in Zhuhai, Guangdong Province, after which its intensity rapidly decreased (Fig. 1a). The duration of Talim's influence on the study area was approximately 1–2 days.

3 Data and method

3.1 Observation data

To study the influence of tropical cyclones on the NSCS coastal upwelling, three sets of fixed-point seabed-based observation systems were set up at water depths of 25.2 m (C1), 22.3 m (C2), and 18.8 m (C3) (Fig. 1), respectively, in the waters off the Shanwei coast, Guangdong. Each seabed-based observation system was equipped with an acoustic wave and acoustic Doppler current (AWAC) profiler, manufactured by Nortek (sampling interval: 5 min; vertical resolution: 0.5–1 m), and a temperature and depth logger (a duo T.D manufactured by RBR Ltd., Canada). A shore-based meteorological observation station (W1) was also set up to observe the wind speed and direction, as well as the air temperature and pressure (Fig. 1). Observations were measured between May 14 and July 3, 2012. During this time period, tropical cyclones Talim and Doksuri passed by the study area (Fig. 1a).

The directions of the coastline and measured currents in the stations of C2 and C3 were both east-westward, whereas the directions of the coastline and measured currents at station C1 were southwestward and northeastward, respectively (Fig. 1b). To facilitate a comparison, the measured currents at each station were decomposed into two components, one parallel to the coastline (u') and the other perpendicular to the coastline (v'), and the coordinate axes of station C1 were rotated 45° counterclockwise; the measured winds at station W1 were also decomposed into two components (along-shore wind and cross-shore wind), and the coordinate axis of station W1 was rotated 45° counterclockwise (Fig. 1b). The measured currents at the three stations were divided into a tidal component (i.e., the tidal currents) and a non-tidal component (i.e., the residual currents) using the T-Tide program package (Pawlowicz et al. 2002). Furthermore, the measured tidal-level data measured at station C2 were divided into a tidal component and a non-tidal component (i.e., the residual water level) as the data quality at station C2 was better than that at stations C1 and C3.

3.2 Satellite remote sensing data

Although the in situ observation data have unique advantages in revealing the long-term evolution of the hydrodynamic environment, they are limited by their geographic location and

only control a relatively small spatial scale; therefore, other observation methods (such as satellite remote sensing) are required to observe large areas. Both the upwelling system and the tropical cyclone process are distributed over a relatively large area and long period. By combining continuous in situ and satellite remote sensing observations, we could achieve more clarity on our study topic of the influence of tropical cyclones on the evolution of an upwelling system (Ye et al. 2013; Sun et al. 2014).

The satellite remote sensing data used in the present study include sea surface temperature (SST), sea surface wind field (SSWF), and sea surface current field (SSCF). The SST data (spatial grid resolution: 0.25°; temporal resolution: 1d) originated from the NOAA optimum interpolation 1/4 degree daily sea surface temperature analysis (<https://rda.ucar.edu/datasets/ds277.7>). The SSWF and SSCF data (spatial resolution: 0.5°; temporal resolution: 1 h) originated from the NCEP Climate Forecast System Version 2 Products (<https://rda.ucar.edu/datasets/ds094.1>). The wind stress and Ekman volume transport during the tropical cyclones processes were calculated based on the downloaded primary wind field data based on previous studies (Trenberth et al. 1990). This study processed the satellite remote sensing data using conventional mature methods. Because the satellite remote sensing data processing algorithms, differences between different algorithms and comparisons between satellite remote sensing and measured data are not the focus of this study, these details are not provided here.

4 Results

4.1 Monthly average SST and SSCF

According to previous studies, the NSCS coast upwelling system is gradually established between May and June, after which its strength gradually increases, reaching its maximum in July, before it starts to decrease in August (Hu et al. 2000; Yang et al. 2002; Su 2004; Zhang et al. 2011). Figure 2 shows the distribution of monthly average SST in the NSCS coastal area between May and August 2012. It can be seen that the SST was low off the NSCS coast in May (Fig. 2a). Starting in June, the SST gradually increased, but the coastal waters did not exhibit the characteristics of upwelling (Fig. 2b). In July, the NSCS coastal water temperature significantly increased with a noticeable upwelling emerging in the Shantou-Dongshan waters and extending in a “tongue-like” manner towards the deep-water area (Fig. 2c). The SST in the upwelling region was 1.0–1.5 °C lower than that in the surrounding waters. Compared to the situation in July, when the development of the upwelling was at its peak, the SST within the earlier upwelling region increased in August, and the area of the upwelling region decreased with the relatively low SST

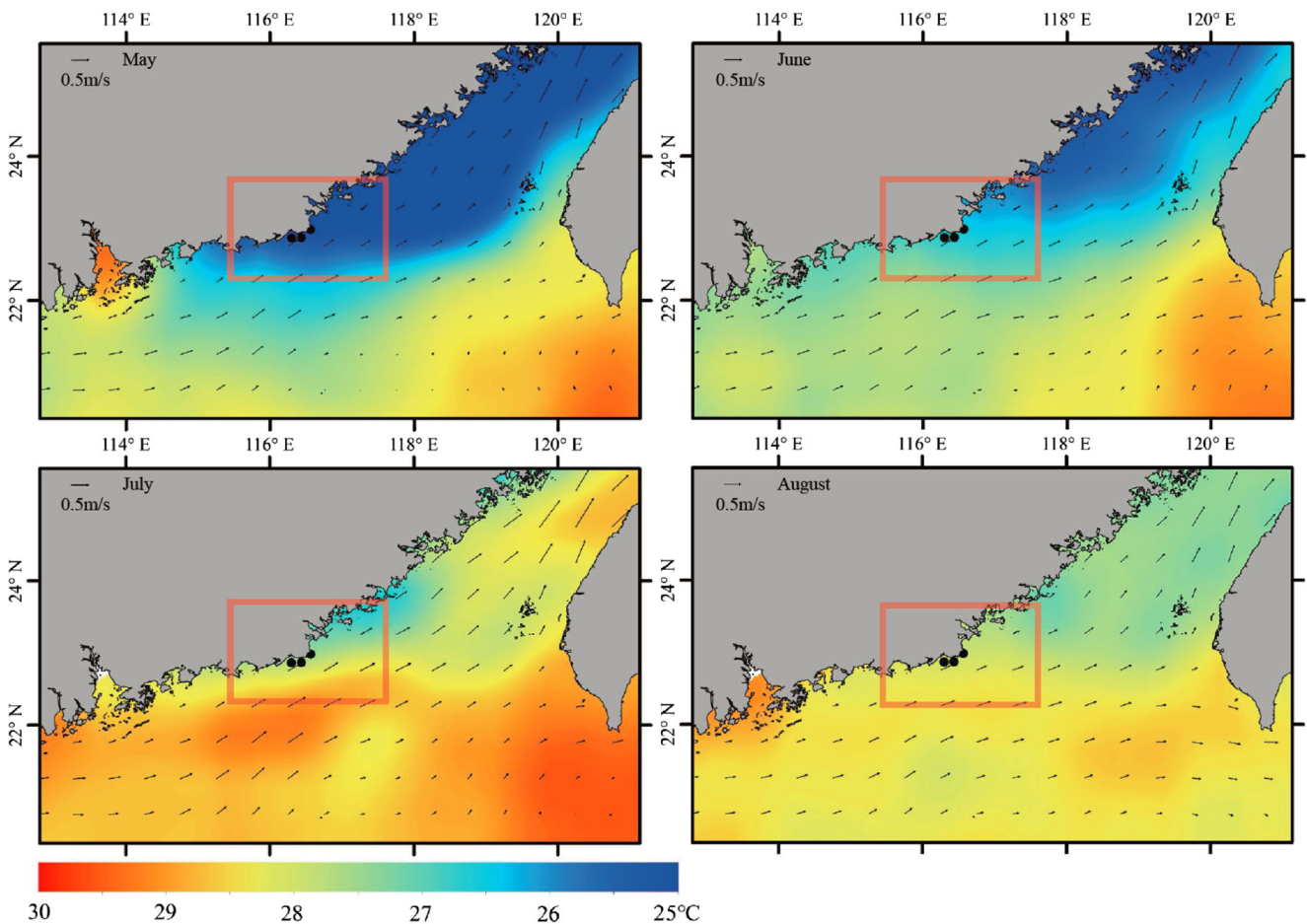


Fig. 2 Monthly average SST distribution color maps and SSCF vectors of the NSCS between May and August 2012. **a** May. **b** June. **c** July. **d** August. The orange boxes signify the study area, and black dots signify the observation stations (C1, C2 and C3). The sign convention is used for the color map

that appeared in the waters near Dongshan Island (Fig. 2d). It can be observed from Fig. 2 that the northeastward current dominated the currents off the NSCS coast during the observation period.

4.2 Local wind field, atmospheric pressure and air temperature

Continuous meteorological data measured at the meteorological station in Shanwei show that a southwesterly to northeasterly wind, with a maximum wind speed of 9.2 m/s (Fig. 3a and T1), was the prevailing wind in the study area when observations began in May. Starting on June 4, the wind speed gradually decreased, and the wind direction gradually became southeasterly. On June 8, a stable southwesterly wind formed with a maximum wind speed of 9.9 m/s, which indicates that the Asian southwest monsoon gradually started to control the study area (T2). Starting on June 12, a northeasterly wind lasted for approximately 3 days because of the effect of a tropical disturbance (T3). After that, the study area was affected by tropical cyclones Talim (maximum wind speed: 8.5 m/s,

northeasterly wind) and Doksuri (maximum wind speed: 8.4 m/s, northeasterly wind) between June 17 and June 20 and between June 28 and June 29, respectively (T4 and T6). The durations of tropical cyclones Talim and Doksuri were approximately 32 and 16 h, respectively, according to the duration time of wind speeds larger than 4.1 m/s, which is the average wind speed between June 8 (when the wind changed back to southwest) and July 3 in the study area.

Accompanying the changes in weather and wind speed, the atmospheric pressure measured in Shanwei Station significantly decreased three times during the tropical disturbance (T2) and the two tropical cyclone (T4 and T6) periods (Fig. 3b). The air temperature at the observation stations exhibited an overall increasing trend at a rate of 0.1 °C/day with the season shift (Fig. 3c).

4.3 Residual water level and bottom water temperature

The residual water level at station C2, excluding the astronomical tidal level, corresponded well to the alongshore wind (Fig. 4a). The warm current of the SCS flows northeastward

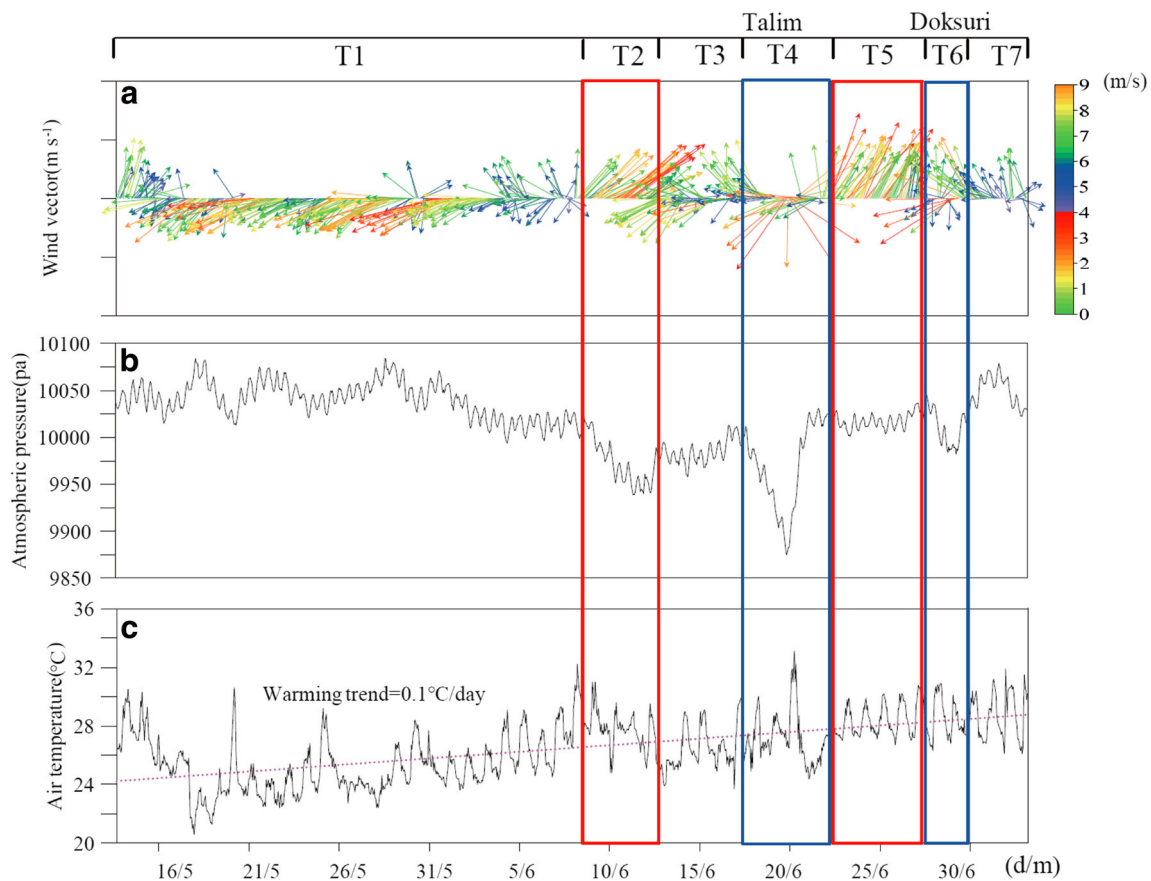


Fig. 3 Variation curves of the **a** wind vector, **b** atmospheric pressure, and **c** temperature data observed at the weather station between May 13 and July 3, 2012. Orange and blue boxes signify the southwesterly wind and tropical cyclones Talim and Doksuri, respectively

along the continental shelf break between the 100- and 200-m isobaths off the Guangdong coast, which is relatively far from our study area and has very limited influence on the water level changes in the study area. According to the theory of Ekman drift (Alvarez et al. 2008), continuous northeasterly winds would lead to a rise in residual water level along the shore in the study area (T1 and T3). The observation data indicate that the maximum residual water level increment reached 0.34 m (T1) and 0.32 m (T3). In comparison, relatively stable southwesterly winds caused the surface seawater to flow away from the shore and the residual water level to drop to a relatively low level. The resulting minimum residual water level was -0.13 m (T2) and -0.25 m (T5), respectively, for predominantly southwesterly winds. The variations in the residual water level varied significantly when tropical cyclones Talim and Doksuri affected the study area (T4 and T6) due to their different routes (Talim passed by the right side of the study area, while Doksuri passed by the left side of the study area). When tropical cyclone Talim (T4) passed by, a significant residual water level reduction occurred at station C2, with a maximum reduction of -0.32 m. When tropical cyclone Doksuri (T6) passed by, a significant residual water level increase occurred, with a maximum increase of 0.25 m.

According to the results of cross spectrum analysis (Lacoss 1971), the variation in residual water level corresponded well

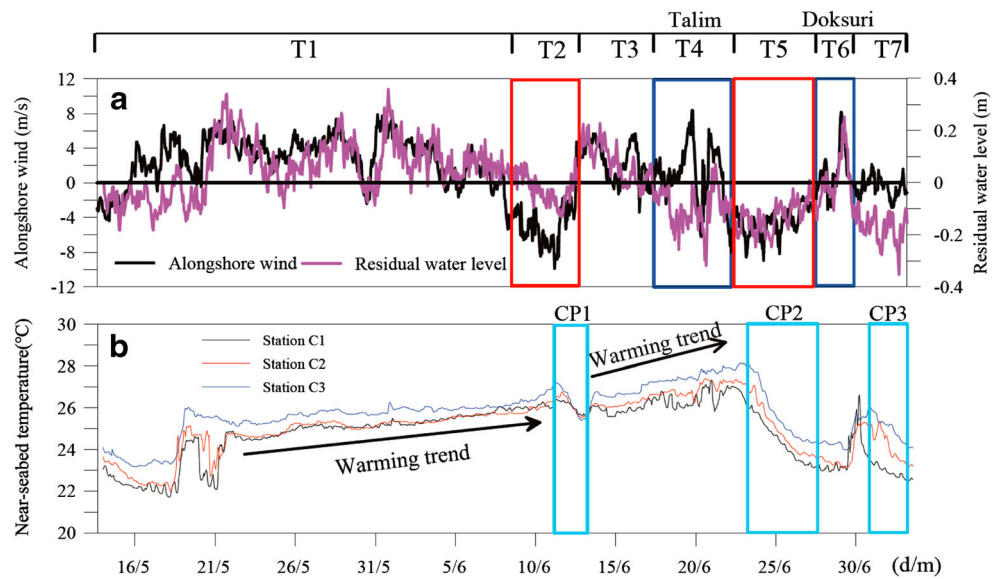
with that of the alongshore wind speed, with a correlation coefficient squared (R^2) (lagged behind approximately 8 h) of 0.37 (Fig. 4a and Table 1). The R^2 values and lag times were significantly different during different periods (Fig. 4a and; Table 1); they were 0.32 and 0.18 and 9 h and 5 h, respectively, during the northeasterly wind period (T1, T3) and 0.41 and 0.60 and 10 h and 9 h, respectively, during the southwesterly wind period (T2, T5). The R^2 was relatively low (0.19) and the lag time was relatively short (6 h) during the tropical cyclone Talim-affected period (T4), and the R^2 increased to 0.54 and the lag time shortened to 3 h during the tropical cyclone Doksuri-affected period (T6).

Between May 18 and June 11, the bottom water temperatures at stations C1, C2 and C3 all exhibited general gradually increasing trends (Fig. 4b). Three noticeable decreases in bottom water temperature (CP1, CP2 and CP3) occurred during the observation period, with the largest decrease of greater than 4 °C occurring between June 23 and 28 during the CP2 event (Fig. 4b).

4.4 Residual currents

The change in the residual coastal currents is also an obvious direct evidence of the formation and evolution of an upwelling.

Fig. 4 Variation curves of the **a** alongshore wind and residual water level, and **b** bottom seawater temperature data obtained at the continuous observation stations between May 13 and July 3, 2012. Orange and blue boxes signify the southwesterly wind, and tropical cyclones Talim and Doksuri, respectively; and (a) light blue boxes (CP1–CP3) signify events when the bottom seawater temperature decreases (b)



The residual currents measured at the three stations were decomposed to components perpendicular and parallel to the coastline (i.e., alongshore and cross-shore components), respectively. Generally, the change of currents in the alongshore direction was greater than that in the cross-shore direction by one order of magnitude (Fig. 5). The near-surface along-shore current was well-correlated to the wind speed and direction measured at station W1 (Fig. 3a). When the wind speed peaked, the near-surface current increased, and vice versa.

During the period when northeasterly winds were the prevailing winds (Fig. 3a and T1), the westward surface alongshore current was significantly enhanced, with the maximum speed exceeding 0.5 m/s (Fig. 5a–e). During the period when southwesterly winds were the prevailing winds (T2 and T5), the eastward surface alongshore current was significantly enhanced, with the maximum speed exceeding 0.4 m/s (Fig. 5a–e). Below the sea surface, the alongshore current speed rapidly decreased, and its change in speed was insignificantly related to the change in wind speed.

While the perpendicular cross-shore currents measured at the three stations changed a small amount, their change was direct evidence of the occurrence and evolution of the upwelling. When southwesterly winds prevailed over the study area (T2 and T5), an obvious onshore current, with a maximum speed of 0.1 m/s, occurred near the bottom water

(Fig. 5b–f), which was direct evidence of the occurrence of the upwelling.

Before tropical cyclone Talim formed (Fig. 5 and T3), the study area was affected by a tropical disturbance, and the wind direction at station W1 turned from southwesterly to northeasterly (Fig. 3a). Correspondingly, the upwelling structure in the water column, which was formed by the effect of the southwest monsoon winds, was destroyed. At this point, the cross-shore currents were manifested in an onshore direction in the surface water and in an offshore direction in the bottom water (Fig. 5b–f), which was unfavorable to the formation of the upwelling.

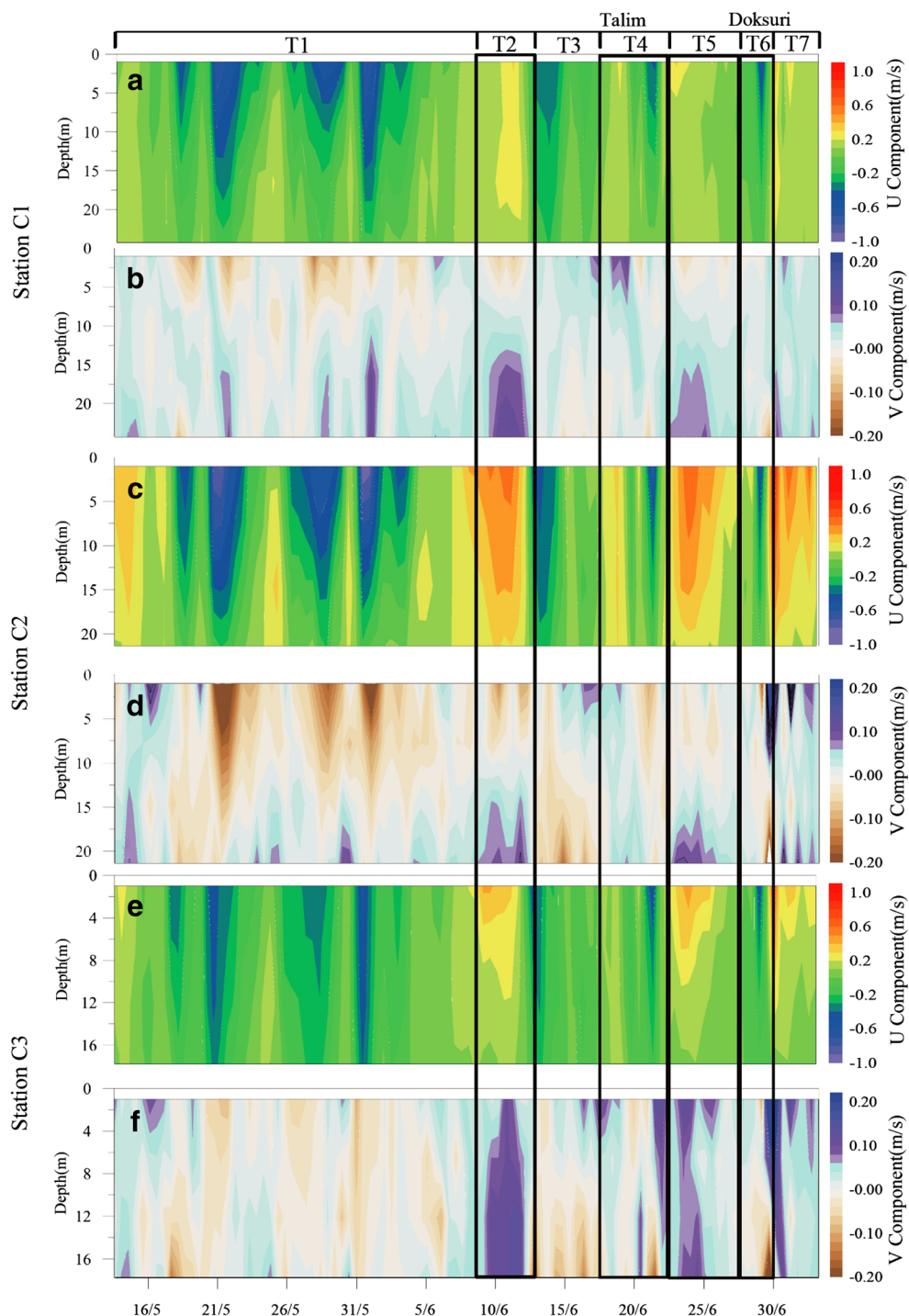
During the period when tropical cyclone Talim affected the study area (T4), as the local wind field changed, the cross-shore current structure was changed to create unfavorable conditions for upwelling formation (Fig. 5b–f). As tropical cyclone Talim passed the study area and dissipated (T5), starting from June 21, the prevailing winds over the study area turned to southwesterly winds, such that the current structure rapidly recovered and noticeable onshore currents emerged near the bottom of the sea, exhibiting the structural characteristics of coastal upwelling.

Compared with Talim, tropical cyclone Doksuri had nearly the same intensity but a completely different moving path and a relative short duration in the study area (T6). Doksuri entered the SCS at 15:00 on June 28. Afterwards, the local wind

Table 1 The correlation coefficients squared (R^2) and lag times of local along-shore wind and residual water level at Station C2

Station	T1~T7		T1		T2		T3	
	R^2	Lag (hours)						
W1/C2	0.37	7	0.32	9	0.45	10	0.18	5
	T4		T5		T6		T7	
	R^2	Lag (hours)						
	0.19	6	0.52	9	0.54	3	0.16	6

Fig. 5 Variations in the U and V components of the residual currents at stations C1 (**a** and **b**), C2 (**c** and **d**) and C3 (**e** and **f**) between May 14 and July 3, 2012 (black boxes signify the southwesterly wind and tropical cyclones Talim and Doksuri)



gradually changed to northeasterly. As tropical cyclone Doksuri came near the study area, the original seasonal upwelling structure was destroyed. After tropical cyclone Doksuri made landfall and dissipated, the local winds turned back to southeastward and then southward, and the cross-shore currents turned into an onshore direction from the surface to the bottom. However, no original seasonal upwelling structure was formed until the end of the observation period (Fig. 5b–f).

The results of wavelet analysis (Torrence and Compo 1998) of the alongshore current (Fig. 6a) show that near-inertial oscillations (Shay et al. 1998) and subinertial waves were triggered (with a period of 48–240 h) during the periods affected by tropical cyclones Talim and Doksuri in Station C2 (Fig. 6b–d). Those subinertial waves were important because they were readily excited and spread the response of the ocean in the alongshore

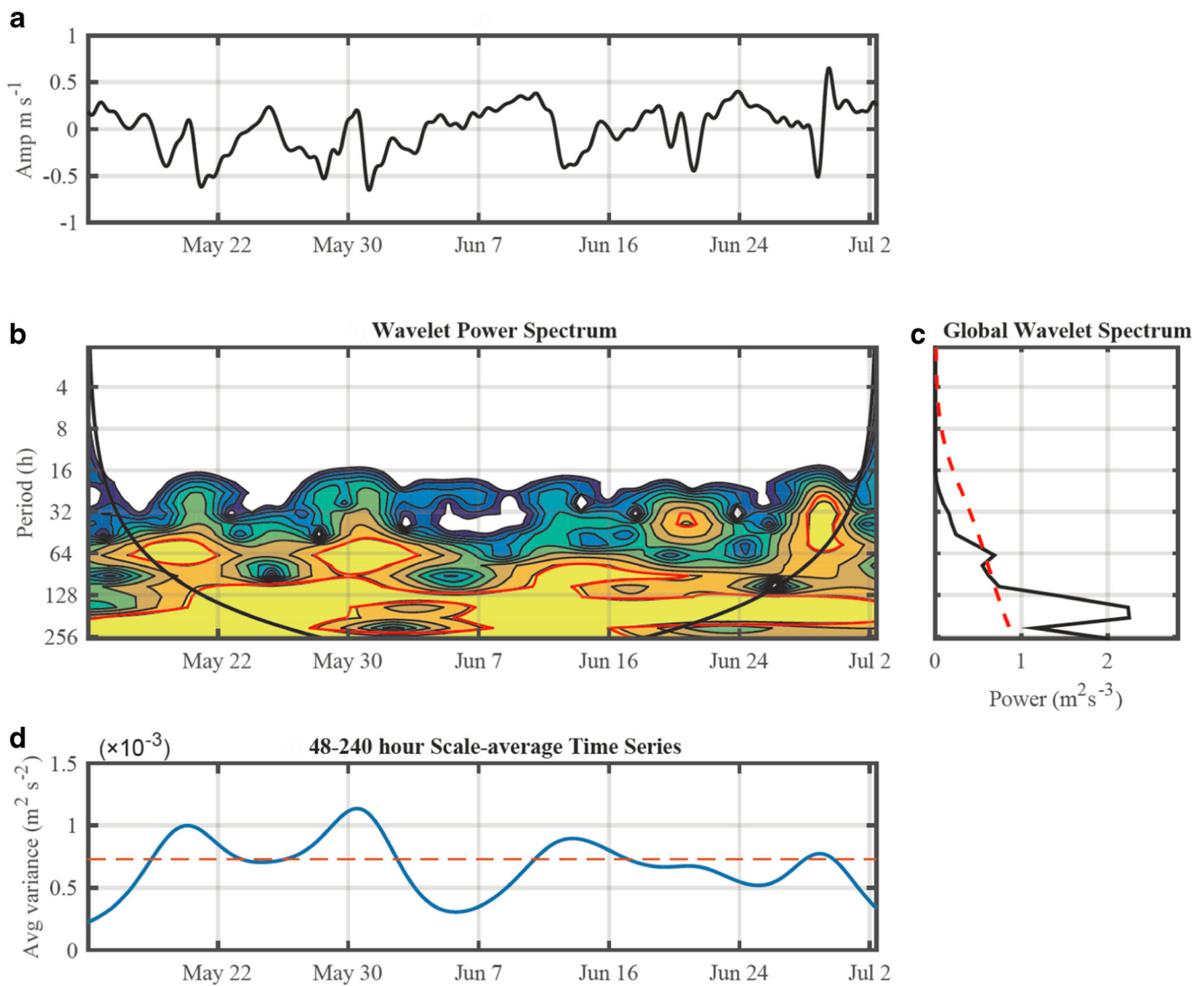


Fig. 6 **a** Vertically averaged along-shore current at station C2. **b** Wavelet power spectrum (Morlet wavelet), where the black line indicates the cone of influence and the red line represents the 95% significance level. **c**

Global wavelet power spectrum, where the red dashed line indicates the 95% significance level. **d** Band-averaged time series for 48–480 h, where the red dashed line indicates the 95% significance level

direction through their propagation by the processes of the tropical cyclones (Shen et al. 2017).

5 Discussion

5.1 Evolution of the upwelling in the coastal waters of the NSCS

Both changes in the ocean cross-shore currents and the rise of the cold bottom seawater are typical signs of the formation and distribution of coastal upwelling (Gan et al. 2005; Pan et al. 2012). Corresponding to the two periods when southwestward winds (upwelling-favorable winds) prevailed over the study area (T2 and T5), a significant residual water level reduction (Fig. 4a), a change in the onshore current velocity of 0.1 m/s

(Fig. 5b–f), and a sharp decrease in the bottom water temperature (Fig. 4b, CP1 and CP2) can be observed in the study area. These phenomena are direct proof of the onshore intrusion of the SCS subsurface water and the formation of upwelling, which are consistent with the results of previous studies (Jing et al. 2009). In comparison, when controlled by upwelling-unfavorable northeasterly winds, the residual water level increased, and offshore currents emerging near the bottom with the bottom water temperature gradually increased (Fig. 4a). In contrast, at the beginning of May to June, the northeastern region of the South China Sea exists in a monsoon transition period; the southwest wind only appears sporadically in some periods, which may cause a short period of upwelling (Figs. 4 and 5b–f).

The seasonal upwelling system in the NSCS coastal area in summer is an important component of the coastal circulation

(Pan et al. 2012). The rapid change in the local wind field within a short period (particularly during an extreme marine weather event) has a significant influence on the stability and development of the seasonal upwelling system. However, from a long-term perspective, the background southwest wind field in the NSCS in summer is still the dominant factor controlling the formation and stable development of the upwelling (Hong et al. 2009; Jing et al. 2009), which is corroborated by the intrusion of the cold bottom water during the observation period (Fig. 4b, CP1, CP2 and CP3).

During the observation period, the most intense intrusion of the cold water occurred between June 23 and June 28 (Fig. 4b and CP2), when the bottom water temperature dropped by approximately 4.1 °C. However, the SST distribution maps of the same period (Fig. 7d–f) show that the SST of the study area was relatively high, and the strength of the upwelling at this time had not reached a sufficient level to allow the cold bottom water to rise to the sea surface.

Under further comparative analysis of the cold water intrusion processes after the two tropical cyclones, we can find that the CP3 event is a continuation of the CP2 event (Fig. 4b, CP2 and CP3), as cyclone Doksuri only destroyed the upwelling system for a short time. Although the local wind fields were different during the two events (CP2 and CP3), the surface current fields were similar, with a strong eastward surface current (off-shore current) (Figs. 5 and 8). This phenomenon proved that the local topography also played an important role in the formation of the upwelling system, which was sensitive to the along-shore current (Wang et al. 2014; Gan et al. 2015), and the upwelling system can be maintained under the condition of the significantly eastward current in the study area and without a local southwest wind field. Therefore, the strong offshore current (eastward current) should be an important contribution to maintaining the coastal upwelling system in the study area (Figs. 5 and 8), while the formation of the eastward current was controlled by the southward wind in the NSCS coastal area (Fig. 8h).

5.2 Impact of tropical cyclones on the upwelling development

Under the influence of the tropical disturbance and tropical cyclones, the original water current structure was disrupted (Fig. 5b–f; T3, T4 and T6), and the summer monsoon-driven upwelling system was also destroyed. Since the study area generally experienced upwelling-favorable conditions during the observation period, the hydrodynamic environment recovered rapidly after being disrupted by the events; therefore, the seasonal upwelling system also recovered quickly.

Before Talim influenced the study area (Fig. 3a and T3), a northeastward wind, which lasted for approximately 3 days as

a tropical disturbance, caused a change in the direction of the currents parallel to the coastal direction (Fig. 5a–e). When Talim approached the study area, the transport changed to unfavorable conditions for upwelling. As Talim moved north-eastward, passed through the Taiwan Strait and then eventually dissipated, the local wind and current fields changed into an unfavorable situation for the recovery of the upwelling system.

After Talim passed by the study area and dissipated, its influence on the study area gradually disappeared accordingly, and the waters were once again controlled by prevailing southwestward winds (Fig. 3a). The coastal current structure gradually recovered to the seasonal upwelling regime. The off-shore transport of surface water and inshore transport of bottom water assisted in the rapid recovery of the upwelling system. This occurred simultaneously with the intrusion of cold bottom water (Fig. 4b, CP2). Since the coastal upwelling system was just established, its strength might be relatively low and not sufficient to allow the cold bottom water to rise to the sea surface. At the same time, the freshwater plume of the Pearl River, with a relatively high temperature, might have had a significant impact on the hydrodynamic environment in the study area by blocking the upwelling of the cold bottom water, being pushed by the southwestward wind, and diffusing northeastward in the water surface of the study area (Fig. 7d–f) (Dong et al. 2004; Gan et al. 2009a, b).

Compared with tropical cyclone Talim, Doksuri had nearly the same intensity, but a different moving path and relatively shorter influence time on the study area. During the period when Doksuri approached the study area, the residual water level increased and the direction of alongshore current shifted (Fig. 5a–e). The seasonal upwelling structure was again reestablished after tropical cyclone Talim was destroyed, and the bottom water temperature increased by approximately 2 °C (Fig. 5b–f). Because the stations were located out of the center of cyclone Doksuri (the level 7 wind circle), the wind in the stations was controlled by the peripheral winds of the cyclone and the influence time of cyclone was relatively shorter than that of cyclone Talim; additionally, the along-shore winds were correlated well with water level, which was different during cyclone Talim (Fig. 4a; Table 1). After Doksuri made landfall and dissipated, upwelling-favorable southwestward winds did not rapidly dominate the study area. However, relatively cold bottom water was observed in all three stations, which demonstrates that the upwelling system was being gradually reestablished in the study area (Fig. 4b and CP3).

The origin, path, speed, intensity, and duration of the two tropical cyclones were significantly different, and as a result, the impacts of the tropical cyclones on the evolution of the upwelling system were different. When cyclone Talim approached the study area, the residual water level was significantly decreased, with a maximum decrease of approximately

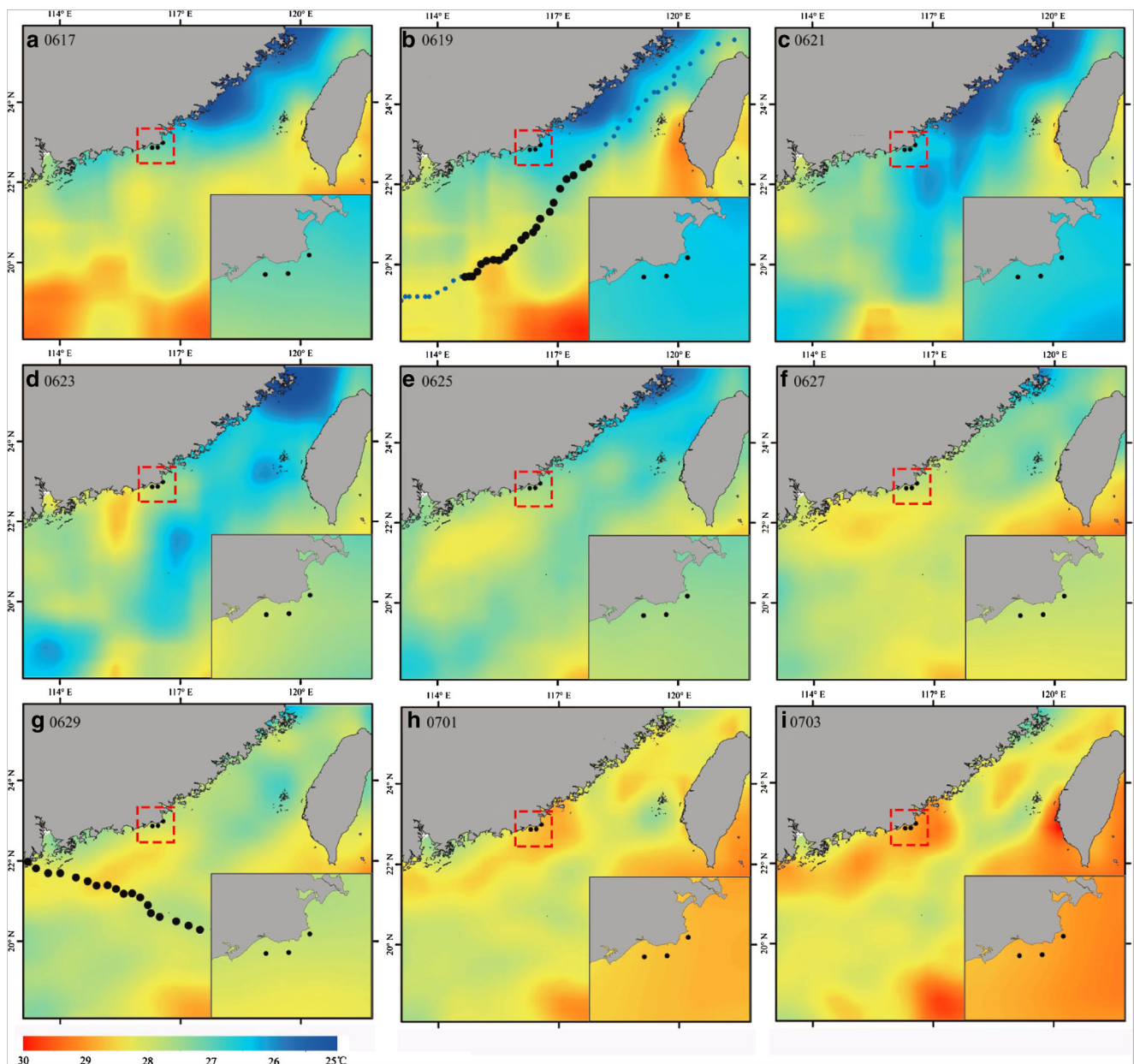


Fig. 7 Daily average SST distribution maps of the NSCS between June 17 and July 3, 2012. Black dots signify the paths of the tropical cyclones

−0.32 m (Fig. 4a and T4), when the local wind shifted to southwest (Fig. 3a) due to the strong Ekman volume transport by the cyclone Talim winds (Fig. 9a) (Trenberth et al. 1990; Alvarez et al. 2008). In the relatively deep sea, an obvious strip-shaped low-temperature water body emerged along the cyclone path due to cyclone-pumping or cyclone-induced water mixing (Fig. 7c–i) (Price 1983). After cyclone Talim passed by, the seasonal upwelling system was formed and maintained under the control of an upwelling-favorable southwestward wind for a relatively long time, until the processes of cyclone Doksuri destroyed the upwelling system. The Ekman volume transport of cyclone Doksuri was significantly lower than that of cyclone Talim (Fig. 9). When cyclone

Doksuri approached the study area, the residual water level was significantly increased (Fig. 4a and T6) due to the relatively low cyclone-pumping effect (Fig. 9b) and the strong cyclone-induced water accretion in the coastal area, and the R^2 increased to 0.54. The seasonal upwelling system was again destroyed by cyclone-induced dynamic processes. After cyclone Doksuri passed by, the upwelling system was soon re-established under the control of an upwelling-favorable eastward surface current (offshore current).

A variety of oceanic responses is generated during the passage of a tropical cyclone, which include subinertial and near-inertial motions and geostrophic balanced motions (Ding et al. 2011; Shen et al. 2017). During the cyclone Talim- and

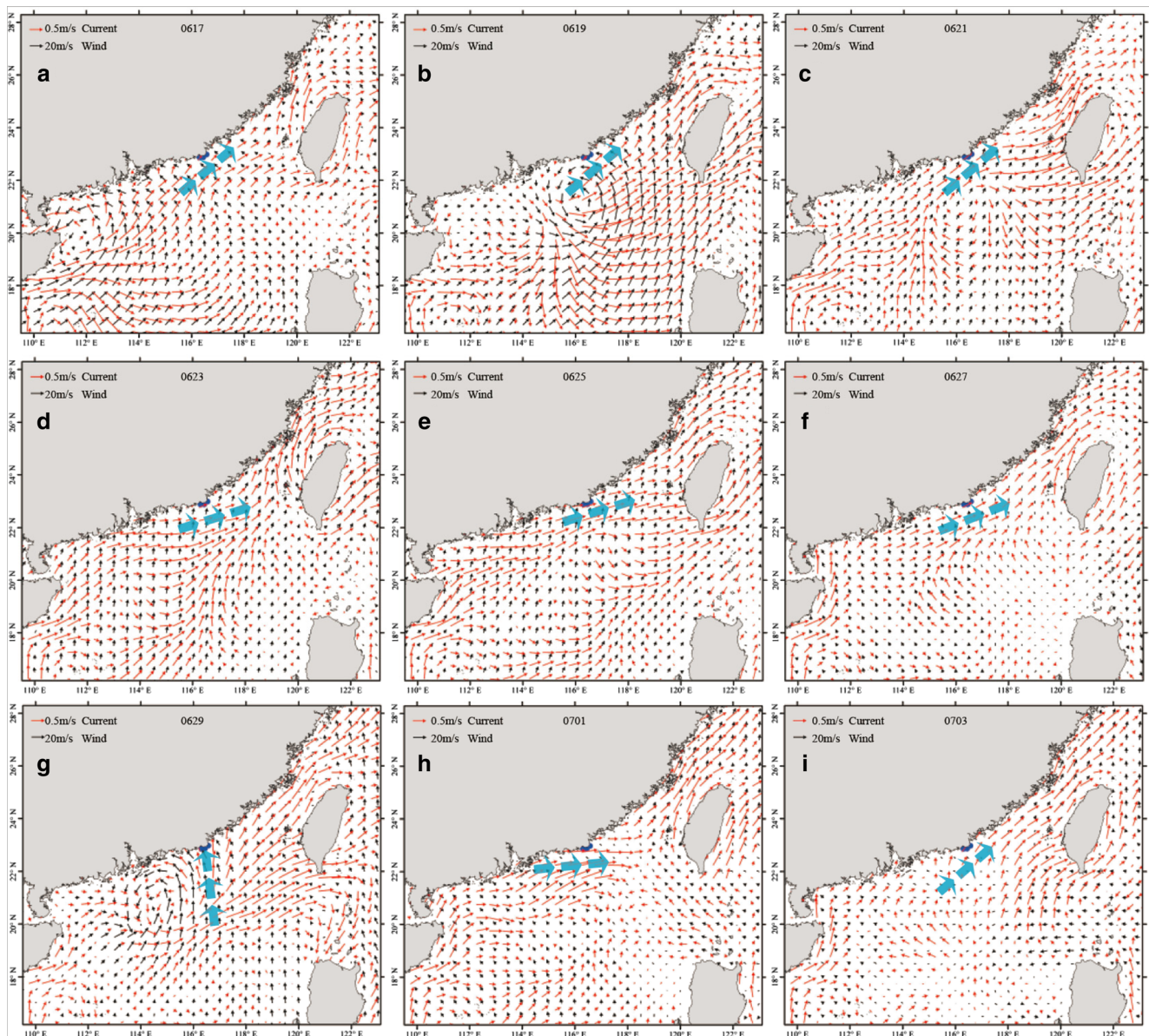


Fig. 8 Planar distribution maps of the sea surface wind field (SSWF) and sea surface current field (SSCF) in the NSCS between June 17 and July 3, 2012 (black and red arrow lines signify the wind and current vectors,

respectively; the blue arrow line signifies the local current vector; and blue dots signify the observation stations (C1, C2 and C3))

Doksuri-affected periods, both the residual water level and currents showed near-inertial oscillations and subinertial waves with periods of 2–10 days (Fig. 6). These oscillations should be aroused by the combined effects of the local wind field and other factors, such as coastal trapped waves (Ding et al. 2011; Li et al. 2015a). The local wind field was relatively stable under normal weather conditions, controlled by the southwest monsoon, in the study area during the observational period. The early local wind field gradually changed under the influence of the tropical cyclones and mainly controlled the wind field in the study area; as a result, the wind was more associated with the residual water decreases in the T2 and T5 time periods. The change in residual water level was mainly

controlled by cyclone-pumping during cyclone Talim and by the peripheral wind field during cyclone Doksuri due to the study area being located in the level 7 wind circle of cyclone Talim and out of the level 7 wind circle of cyclone Doksuri. Therefore, the upwelling system was completely destroyed by cyclone Talim (with a low R^2 value, 0.19), while it was only slightly disrupted and rapidly recovered during cyclone Doksuri (with a high R^2 value, 0.54) (Table 1).

The results of the present study demonstrate that tropical cyclones have a significant impact on the upwelling system in the NSCS coastal area. However, limited by the location of the stations and the observation time, the present study could not comprehensively reveal the complete mechanism by which a

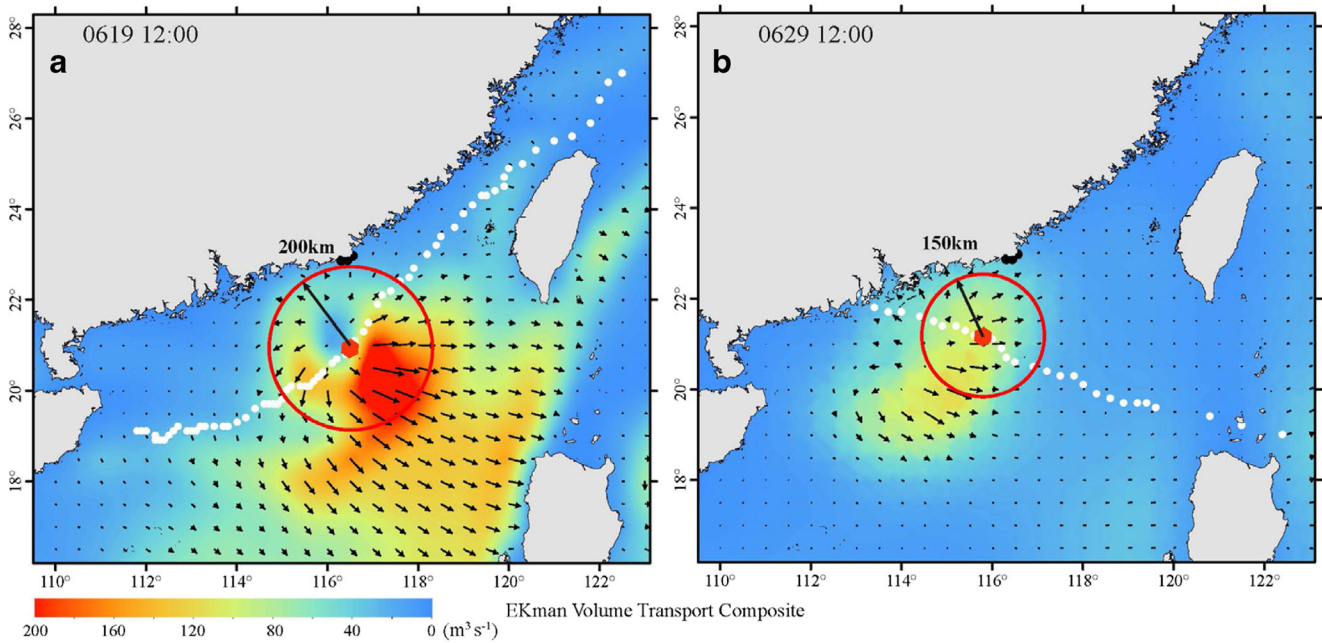


Fig. 9 Planar distribution maps of Ekman volume transport in the study area during tropical cyclones Talim (a) and Doksuri (b). Black dots signify the location of each bottom-supported seabed base observation

station (C1, C2 and C3); white dots signify the paths of tropical cyclones Talim and Doksuri; and red lines signify the level 7 wind circle radii of tropical cyclones Talim and Doksuri

tropical cyclone affects the upwelling system and its evolution, as well as the difference in impact between tropical cyclones varying in path, intensity, and speed. Long-term multi-parameter continuous observations at key locations of an upwelling, combined with mathematical modeling, are an effective means of accurately understanding these topics. These observations are important and require urgent implementation in both the present study area and other sea areas where upwelling develops.

6 Conclusion

This study investigates the evolution of the monsoon-driven upwelling system in the coastal area of the NSCS during the passage of two tropical cyclones using continuous ocean and atmospheric observations data, as well as satellite sensing data. The following conclusions are obtained:

- (1) The variations in local along-shore winds, coastal residual water level, and currents corresponded well in the NSCS coastal area. The development of upwelling in the study area is mainly controlled by the Asian southwest monsoon, and the eastward current also plays an important role in maintaining the upwelling system, especially after tropical cyclone processes. The variations in alongshore wind will induce variations in the local residual water level and currents within 1 day, thus influencing the upwelling intensity.

- (2) Tropical cyclones have a significant impact on the upwelling system by changing the local wind and current fields. The oscillations of local residual water level and currents are aroused by the combined effects of local wind field and other factors, such as near-inertial oscillations and subinertial waves, during tropical cyclones. The hydrodynamic environment of the upwelling system will rapidly recover to normal sea conditions after the cyclone passes due to the relatively short duration of the impact of a tropical cyclone on the dynamic environment of the waters.

More research, such as mooring observations in key locations, is urgently needed to reveal the complicated processes of the evolution of upwelling and the impact of tropical cyclones on this evolution.

Acknowledgments We thank all of the investigators for their help in collecting data during the observations. This work was supported by the National Science Foundation of China (NSFC, Grant nos. 41676028, 41276059), the Scientific Research Foundation of the Third Institute of Oceanography, SOA (Grant nos. TIO2014016, TIO2013026) and the National Programme on Global Change and Air-Sea Interaction (No. GASI-GEOGE-03). This manuscript benefited from comments by the editor and two anonymous reviewers.

References

Allen JS (1973) Upwelling and coastal jets in a continuously stratified ocean. *J Phys Oceanogr* 3(3):245–257. [https://doi.org/10.1175/1520-0485\(1973\)003<0245:UACJIA>2.0.CO;2](https://doi.org/10.1175/1520-0485(1973)003<0245:UACJIA>2.0.CO;2)

- Alvarez I, Gomez-Gesteira M, de Castro M, Novoa EM (2008) Ekman transport along the Galician Coast (NW, Spain) calculated from QuikSCAT winds. *J Marine Syst* 72(1):101–115. <https://doi.org/10.1016/j.jmarsys.2007.01.013>
- Arthur RS (1965) On calculation of vertical motion in eastern boundary currents from determinations of horizontal motion. *J Geophys Res* 70(12):2799–2803. <https://doi.org/10.1029/JZ070i012p02799>
- Cai WJ, Lennon GW (1988) Upwelling in the Taiwan Strait in response to wind stress, ocean circulation and topography. *Estuar Coast Shelf Sci* 26:15–31. [https://doi.org/10.1016/0272-7714\(88\)90009-1](https://doi.org/10.1016/0272-7714(88)90009-1)
- Chang YH, Liao T, Lee MA, Chan JW, Shieh WJ, Lee KT, Wang GH, Lan YC (2008) Multisatellite observation on upwelling after the passage of Typhoon Hai-Tang in the southern East China Sea. *Geophys Res Lett* 35(3), n/a-n/a. doi:<https://doi.org/10.1029/2007gl032858>
- Chang YC, Tseng RS, Centurioni LR (2010) Typhoon-induced strong surface flows in the Taiwan Strait and Pacific. *J Oceanogr* 66(2): 175–182. <https://doi.org/10.1007/s10872-010-0015-y>
- Chao SY, Shaw PT, Wang J (1995) Wind relaxation as a possible cause of the South China Sea warm current. *J Oceanogr* 51(1):111–132. <https://doi.org/10.1007/BF02235940>
- Chen CTA, Liu CT, Chuang WS, Yang YJ, Shiah FK, Tang TY, Chung SW (2003) Enhanced buoyancy and hence upwelling of subsurface Kuroshio waters after a typhoon in the southern East China Sea. *J Marine Syst* 42(1–2):65–79. [https://doi.org/10.1016/S0924-7963\(03\)00065-4](https://doi.org/10.1016/S0924-7963(03)00065-4)
- Chen ZY, Yan XH, Jiang YW (2014) Coastal cape and canyon effects on wind-driven upwelling in northern Taiwan Strait. *J Geophys Res* 119(7):4605–4625. <https://doi.org/10.1002/2014JC009831>
- Chung CC, Gong GC, Hung CC (2012) Effect of typhoon Morakot on microphytoplankton population dynamics in the subtropical Northwest Pacific. *Mar Ecol Prog Ser* 448(1):39–49. <https://doi.org/10.3354/meps09490>
- Ding Y, Yu H, Bao X, Kuang L, Wang C, Wang W (2011) Numerical study of the barotropic responses to a rapidly moving typhoon in the East China Sea. *Ocean Dynam* 61(9):1237–1259. <https://doi.org/10.1007/s10236-011-0436-1>
- Dong LX, Su JL, Wong LA, Cao ZY, Chen JC (2004) Seasonal variation and dynamics of Pearl River plume. *Cont Shelf Res* 24(16):1761–1777. <https://doi.org/10.1016/j.csr.2004.06.006>
- Fréon P, Barange M, Aristegui J (2009) Eastern boundary upwelling ecosystems: integrative and comparative approaches. *Prog Oceanogr* 83(1–4):1–14. <https://doi.org/10.1016/j.pocean.2009.08.001>
- Gan JP, Allen JS (2002) A modeling study of shelf circulation off northern California in the region of the coastal ocean dynamics experiment, response to relaxation of upwelling. *J Geophys Res* 107(C9): 3123. <https://doi.org/10.1029/2000JC000768>
- Gan JP, Allen JS, Samelson RM (2005) On open boundary conditions for a limited-area coastal model off Oregon. Part 2: response to wind forcing from a regional mesoscale atmospheric model. *Ocean Model* 8(1):155–173. <https://doi.org/10.1016/j.ocemod.2003.12.007>
- Gan JP, Anson A, Guo XG, Li L (2009a) Intensified upwelling over a widened shelf in the northeastern South China Sea. *J Geophys Res* 114(C9):C09019. <https://doi.org/10.1029/2007JC004660>
- Gan JP, Li L, Wang DX, Guo XG (2009b) Interaction of a river plume with coastal upwelling in the northeastern South China Sea. *Cont Shelf Res* 29(4):728–740. <https://doi.org/10.1016/j.csr.2008.12.002>
- Gan JP, Wang JJ, Liang LL, Li L, Guo XG (2015) A modeling study of the formation, maintenance, and relaxation of upwelling circulation on the northeastern South China Sea shelf. *Deep-Sea Res II* 117:41–52. <https://doi.org/10.1016/j.dsr2.2013.12.009>
- Gu YZ, Pan JY, Lin H (2012) Remote sensing observation and numerical modeling of an upwelling jet in Guangdong coastal water. *J Geophys Res* 117(C8):C08019. <https://doi.org/10.1029/2012JC007922>
- Guan BX, Fang G (2006) Winter counter-wind currents off the southeastern China coast: a review. *J Oceanogr* 62(1):1–24. <https://doi.org/10.1007/s10872-006-0028-8>
- Hein H, Hein B, Pohlmann T, Long BH (2013) Inter-annual variability of upwelling off the South-Vietnamese coast and its relation to nutrient dynamics. *Glob Planet Chang* 110(Part B):170–182. <https://doi.org/10.1016/j.gloplacha.2013.09.009>
- Hong HS, Zhang CY, Shang SL, Huang BQ, Li YH, Li XD, Zhang SM (2009) Interannual variability of summer coastal upwelling in the Taiwan Strait. *Cont Shelf Res* 29(2):479–484. <https://doi.org/10.1016/j.csr.2008.11.007>
- Hu JY, Wang XH (2016) Progress on upwelling studies in the China seas. *Rev Geophys* 54(3):653–673. <https://doi.org/10.1002/2015RG000505>
- Hu JY, Kawamura H, Hong HS, Qi YQ (2000) A review on the currents in the South China Sea: seasonal circulation, South China Sea warm current and Kuroshio intrusion. *J Oceanogr* 56(6):607–624. <https://doi.org/10.1023/A:1011117531252>
- Jaimes B, Shay LK (2015) Enhanced wind-driven downwelling flow in warm oceanic eddy features during the intensification of tropical cyclone Isaac (2012): observations and theory. *J Phys Oceanogr* 45(6):1667–1689. <https://doi.org/10.1175/JPO-D-14-0176.1>
- Jaimes B, Shay LK, Brewster JK (2016) Observed air-sea interactions in tropical cyclone Isaac over loop current mesoscale eddy features. *DYNAM ATMOS OCEANS*, 76(part 2):306–324. doi:<https://doi.org/10.1016/j.dynatmoce.2016.03.001>
- Jiang YW, Chai F, Wan ZW, Zhang X, Hong HS (2011) Characteristics and mechanisms of the upwelling in the southern Taiwan Strait: a three-dimensional numerical model study. *J Oceanogr* 67(6):699–708. <https://doi.org/10.1007/s10872-011-0080-x>
- Jing ZY, Qi YQ, Hua ZL, Zhang H (2009) Numerical study on the summer upwelling system in the northern continental shelf of the South China Sea. *Cont Shelf Res* 29(2):467–478. <https://doi.org/10.1016/j.csr.2008.11.008>
- Kuo NJ, Zheng QA, Ho CR (2004) Response of Vietnam coastal upwelling to the 1997–1998 ENSO event observed by multisensor data. *Remote Sens Environ* 89(1):106–115. <https://doi.org/10.1016/j.rse.2003.10.009>
- Lacoss RT (1971) Data adaptive spectral analysis methods. *Geophysics* 36(4):661–675. <https://doi.org/10.1190/1.1440203>
- Li YH, Wang AJ, Qiao L, Fang JY, Chen J (2012) The impact of typhoon Morakot on the modern sedimentary environment of the mud deposition center off the Zhejiang-Fujian coast, China. *Cont Shelf Res* 37(2):92–100. <https://doi.org/10.1016/j.csr.2012.02.020>
- Li YH, Ye X, Wang AJ, Li HD, Chen J, Qiao L (2013) Impact of typhoon Morakot on chlorophyll *a* distribution on the inner shelf of the East China Sea. *Mar Ecol Prog Ser* 483(1):19–29. <https://doi.org/10.3354/meps10223>
- Li JY, Zheng QA, Hu JY, Fan ZH, Zhu J, Chen T, Zhu BL, Xu Y (2015a) Wavelet analysis of coastal trapped waves along the China coast generated by winter storms in 2008. *Acta Oceanol Sin* 34(11):22–31. <https://doi.org/10.1007/s13131-015-0701-0>
- Li YH, Li DY, Fang JY, Yin XJ, Li HD, Hu WY, Chen J (2015b) Impact of typhoon Morakot on suspended matter size distributions on the East China Sea inner shelf. *Cont Shelf Res* 101:47–58. <https://doi.org/10.1016/j.csr.2015.04.007>
- Lin II, Liu WT, Wu CC, Wong GT, Hu C, Chen Z, Liang WD, Yang Y, Liu KK (2003) New evidence for enhanced ocean primary production triggered by tropical cyclone. *Geophys Res Lett* 30(13):1718. <https://doi.org/10.1029/2003GL017141>
- Lin YH, Fang MC, Hwung HH (2010) Transport reversal due to typhoon Krosa in the Taiwan Strait. *Open Ocean Eng J* 3(1):143–157. <https://doi.org/10.2174/1874835X01003010143>
- Lü XG, Qiao FL, Wang GS, Xia CS, Yuan YL (2008) Upwelling off the west coast of Hainan Island in summer: Its detection and

- mechanisms. *Geophys Res Lett* 35(2), n/a-n/a. doi:<https://doi.org/10.1029/2007GL032440>
- Lu ZM, Gan JP, Dai MH, Cheung AYY (2010) The influence of coastal upwelling and a river plume on the subsurface chlorophyll maximum over the shelf of the northeastern South China Sea. *J Marine Syst* 82(1–2):35–46. <https://doi.org/10.1016/j.jmarsys.2010.03.002>
- Mazzini PLF, Barth JA (2013) A comparison of mechanisms generating vertical transport in the Brazilian coastal upwelling regions. *J Geophys Res* 118(11):5977–5993. <https://doi.org/10.1002/2013JC008924>
- Niiler PP (1969) On the Ekman divergence in an oceanic jet. *J Geophys Res* 74(28):7048–7052. <https://doi.org/10.1029/JC074i028p07048>
- Pan AJ, Guo XG, Xu JD, Huang J, Wan XF (2012) Responses of Guangdong coastal upwelling to the summertime typhoons of 2006. *Sci China Earth Sci* 55(3):495–506. <https://doi.org/10.1007/s11430-011-4321-z>
- Pawlowicz R, Beardsley B, Lentz S (2002) Classical tidal harmonic analysis including error estimates in MATLAB using T_TIDE. *Comput Geosci* 28(8):929–937. [https://doi.org/10.1016/S0098-3004\(02\)00013-4](https://doi.org/10.1016/S0098-3004(02)00013-4)
- Price JF (1983) Internal wave wake of a moving storm. Part I: scales, energy budget, and observations. *J Phys Oceanogr* 13(6):949–965. [https://doi.org/10.1175/1520-0485\(1983\)013<0949:IWWOAM>2.0.CO;2](https://doi.org/10.1175/1520-0485(1983)013<0949:IWWOAM>2.0.CO;2)
- Pringle JM (2002) Enhancement of wind-driven upwelling and downwelling by alongshore bathymetric variability. *J Phys Oceanogr* 32(11):3101–3112. [https://doi.org/10.1175/1520-0485\(2002\)032<3101:EOWDUA>2.0.CO;2](https://doi.org/10.1175/1520-0485(2002)032<3101:EOWDUA>2.0.CO;2)
- Shang SL, Zhang CY, Hong HS, Shang SP, Chai F (2004) Short-term variability of chlorophyll associated with upwelling events in the Taiwan Strait during the southwest monsoon of 1998. *Deep-Sea Res II* 51(10–11):1113–1127. <https://doi.org/10.1016/j.dsr2.2004.04.003>
- Shay LK, Mariano AJ, Jacob SD, Ryan EH (1998) Mean and near-inertial ocean current response to hurricane Gilbert. *J Phys Oceanogr* 28(5):858–889. [https://doi.org/10.1175/1520-0485\(1998\)028<0858:MANIOC>2.0.CO;2](https://doi.org/10.1175/1520-0485(1998)028<0858:MANIOC>2.0.CO;2)
- Shen JQ, Qiu Y, Zhang SW, Kuang FF (2017) Observation of tropical cyclone-induced shallow water currents in Taiwan Strait. *J Geophys Res* 122(6):5005–5021. <https://doi.org/10.1002/2017JC012737>
- Su JL (2004) Overview of the South China Sea circulation and its influence on the coastal physical oceanography outside the Pearl River estuary. *Cont Shelf Res* 24(16):1745–1760. <https://doi.org/10.1016/j.csr.2004.06.005>
- Su J, Wang J, Pohlmann T, Xu DF (2011) The influence of meteorological variation on the upwelling system off eastern Hainan during summer 2007–2008. *Ocean Dyn* 61(6):717–730. <https://doi.org/10.1007/s10236-011-0404-9>
- Sun QY, Tang DL, Legendre L, Shi P (2014) Enhanced sea-air CO₂ exchange influenced by a tropical depression in the South China Sea. *J Geophys Res* 119(10):6792–6804. <https://doi.org/10.1002/2014JC010131>
- Tang DL, Kester DR, Ni IH, Kawamura H, Hong HS (2002) Upwelling in the Taiwan Strait during the summer monsoon detected by satellite and shipboard measurements. *Remote Sens Environ* 83(3):457–471. [https://doi.org/10.1016/S0034-4257\(02\)00062-7](https://doi.org/10.1016/S0034-4257(02)00062-7)
- Tee KT, Smith PC, Lefaivre D (1993) Topographic upwelling off southwest Nova Scotia. *J Phys Oceanogr* 23(8):1703–1726. [https://doi.org/10.1175/1520-0485\(1993\)023<1703:TUOSNS>2.0.CO;2](https://doi.org/10.1175/1520-0485(1993)023<1703:TUOSNS>2.0.CO;2)
- Torrence C, Compo GP (1998) A practical guide to wavelet analysis. *Bull Am Meteorol Soc* 79(1):61–78. [https://doi.org/10.1175/1520-0477\(1998\)079<0061:APGTWA>2.0.CO;2](https://doi.org/10.1175/1520-0477(1998)079<0061:APGTWA>2.0.CO;2)
- Trenberth KE, Large WG, Olson JG (1990) The mean annual cycle in global ocean wind stress. *J Phys Oceanogr* 20(11):1742–1760. [https://doi.org/10.1175/1520-0485\(1990\)020<1742:TMACIG>2.0.CO;2](https://doi.org/10.1175/1520-0485(1990)020<1742:TMACIG>2.0.CO;2)
- Wang GH, Ling Z, Wang CZ (2009) Influence of tropical cyclones on seasonal ocean circulation in the South China Sea. *J Geophys Res* 114(C10):C10022. <https://doi.org/10.1029/2009JC005302>
- Wang DX, Hong B, Gan JP, Xu HZ (2010) Numerical investigation on propulsion of the counter-wind current in the northern South China Sea in winter. *Deep-Sea Res I* 57(10):1206–1221. <https://doi.org/10.1016/j.dsr.2010.06.007>
- Wang DX, Shu TQ, Xue HJ, Hu JY, Chen J, Zhuang W, Zu TT, Xu JD (2014) Relative contributions of local wind and topography to the coastal upwelling intensity in the northern South China Sea. *J Geophys Res* 119(4):2550–2567. <https://doi.org/10.1002/2013JC009172>
- Xue HJ, Chai F, Pettigrew N, Xu DY, Shi MC, Xu JP (2004) Kuroshio intrusion and the circulation in the South China Sea. *J Geophys Res* 109(C2):C02017. <https://doi.org/10.1029/2002JC001724>
- Yang HJ, Liu QY, Liu ZY, Wang DX, Liu XB (2002) A general circulation model study of the dynamics of the upper ocean circulation of the South China Sea. *J Geophys Res* 107(C7):3085. <https://doi.org/10.1029/2001JC001084>
- Ye HJ, Sui Y, Tang DL, Afanasyev YD (2013) A subsurface chlorophyll bloom induced by typhoon in the South China Sea. *J Marine Syst* 128(7):138–145. <https://doi.org/10.1016/j.jmarsys.2013.04.010>
- Zhang WZ, Hong HS, Shang SP, Yan XH, Chai F (2009) Strong southward transport events due to typhoons in the Taiwan Strait. *J Geophys Res* 114(C11):C11013. <https://doi.org/10.1029/2009JC005372>
- Zhang CY, Hong HS, Hu CM, Shang SL (2011) Evolution of a coastal upwelling event during summer 2004 in the southern Taiwan Strait. *Acta Oceanol Sin* 30(1):1–6. <https://doi.org/10.1007/s13131-011-0084-9>
- Zhang WZ, Hong HS, Shang SP, Yan XH (2013) Typhoons enhancing northward transport through the Taiwan Strait. *Cont Shelf Res* 56(2):13–25. <https://doi.org/10.1016/j.csr.2013.01.019>
- Zheng GM, Tang DL (2007) Offshore and nearshore chlorophyll increases induced by typhoon winds and subsequent terrestrial rainwater runoff. *Mar Ecol Prog Ser* 333(1):61–74. <https://doi.org/10.3354/meps333061>